Modeling and simulation of DC glow discharges in the AlGaSb -coupled Ar/H₂ hybrid micro plasma system

Hibrit AlGaSb-Ar/H₂ mikro plazma sisteminde DC glow deşarjlarının modellenmesi ve simülasyonu

Authors: *Erhan ONGUN[1], Selçuk UTAŞ[2], Hatice Hilal YÜCEL (KURT)[3], Aybaba HANÇERLİOĞULLARI[4]*

ORCID[1]: 0009-0007-4966-1044

ORCID[2]: 0000-0002-9709-516X

ORCID[3]: 0000-0002-1277-5204

ORCID[4]: 0000-0001-9830-4226

Modeling and Simulation of DC Glow Discharges in the AlGaSb -coupled Ar/H$_2$ Hybrid Micro Plasma System

Highlights

❖ *Sub-atmospheric DC -driven microplasma–semiconductor hybrid system is simulated in 2D media.*

❖ *Spatiotemporal discharge dynamics are highly dependent on the cathode material and gas medium.*

❖ *GDSµPS cell can be regulated by hydrogen addition to argon discharge medium.*

Graphical Abstract

The numerical calculations reveal the spatiotemporal characteristics of 2D -modeled gas discharge-semiconductor microplasma system (GDSµPS) as shown in figure below.
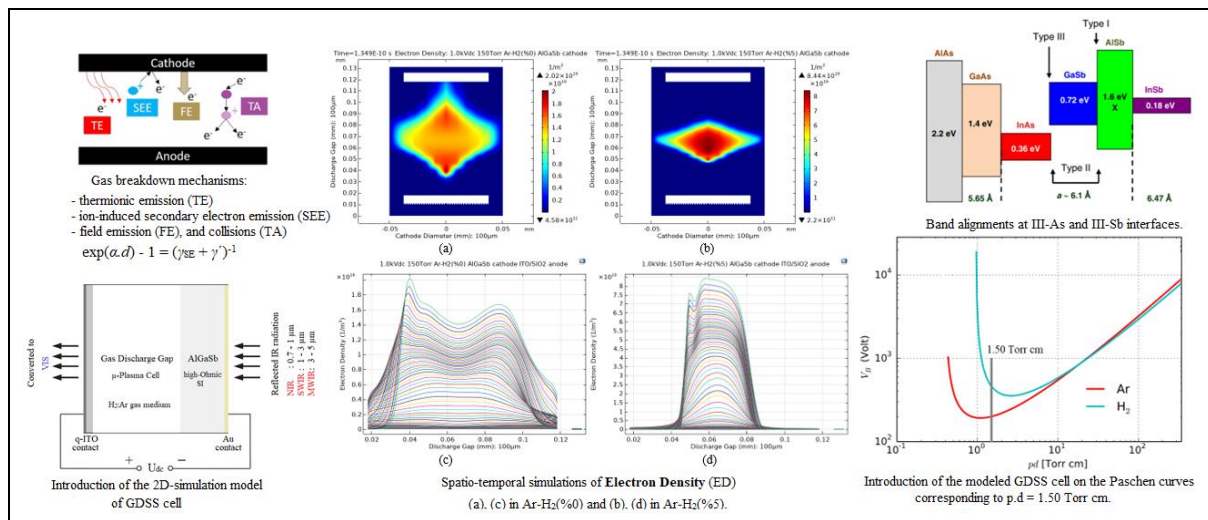
Figure. Introduction of the 2D-GDSµPS cell model and the spatiotemporal simulation results

Aim

It is aimed to investigate the spatiotemporal discharge dynamics of DC -driven microplasma-semiconductor system with surface-modified (digitated) AlGaSb cathode -coupled Ar/H$_2$ gas medium.

Design & Methodology

Numerical analyses of GDSµPS cell were carried out using FEM solver COMSOL Multiphysics program based on mixture-averaged diffusion-drift theory of gas discharges and Maxwellian electron energy distribution function.

Originality

This study is an original research due to the simulation technique and the model solely used to investigate the spatiotemporal discharge characteristics of the 2D-GDSµPS cell, which is uniquely composed of digitated AlGaSb cathode coupled argon-hydrogen gas discharge medium.

Findings

In the gas discharge medium of argon mixed with a molar fraction of 5% hydrogen compared to that of argon with no hydrogen addition, the operating point of GDSµPS cell is shifted upward on the imaginary vertical projection line corresponding to 1.50 Torr.cm as shown on the Paschen curves while the electron energy appears to be denser and more localized across discharge gap of Ar/H$_2$(%5) than that of Ar/H$_2$(%0).

Conclusion

It is concluded that cathode surface modification in microscale can be utilized as an effective design tool to manipulate the key discharge parameters. With hydrogen addition to argon medium, the operating characteristics of GDSµPS cell can be precisely regulated to respond the application-specific requirements.

Declaration of Ethical Standards

The authors of this article declare that the materials and methods used in this study do not require ethical committee permission and/or legal-special permission.

Modeling and Simulation of DC Glow Discharges in the AlGaSb -coupled Ar/H$_2$ Hybrid Micro Plasma System

Araştırma Makalesi / Research Article

Erhan ONGUN[1], Selçuk UTAŞ[2], Hatice Hilal YÜCEL (KURT)[3], Aybaba HANÇERLİOĞULLARI[4*]

[1,2,3*]Gazi University, Graduate School of Natural and Applied Sciences, Department of Physics, Ankara, Türkiye

[4]Kastamonu University, Faculty of Arts and Sciences, Department of Physics, Kastamonu, Türkiye

ABSTRACT

Several studies have been reported on the theoretical and experimental investigation of gas discharge-semiconductor microplasma systems (GDSµPS). In this study, a two-dimensional fluid model of a micro plasma in a square direct current (DC) glow-discharge chamber is simulated using the finite-element method (FEM) solver COMSOL Multiphysics program based on mixture-averaged diffusion-drift theory of gas discharges and Maxwellian electron energy distribution function. A unique III-antimonide high-Ohmic semi-insulating aluminum gallium antimonide (AlGaSb) with finely digitated electron emission surface is modeled as planar cathode electrode coupled to ITO/SiO$_2$ planar anode electrode across a gas discharge gap of 100 µm distance. Argon (Ar) and argon mixed with a molar fraction of 5% hydrogen (Ar/H$_2$) gas media are seperately introduced to the micro gap at sub-atmospheric pressure of 150 Torr, and the cell is driven at 1.0 kV DC by a stationary power source to simulate the transitions from electron field emission state to self-sustained normal glow discharge state.The model is simulated to exhibit the transient physical characteristics of the AlGaSb-Ar/H$_2$ glow-discharge micro plasma system by solving the spatiotemporal dynamics of various discharge parameters including, electron density, electron energy density, electron current density and electric potential. It has been observed that a fraction of hydrogen addition to argon can be used as an effective tool in modeling application-specific hybrid micro plasma–semiconductor based infrared photodetector devices.

Key words: Microplasma, AlGaSb, DC plasma simulation, infrared photodetector.

Hibrit AlGaSb-Ar/H$_2$ Mikro Plazma Sisteminde DC Glow Deşarjlarının Modellenmesi ve Simülasyonu

ÖZ

Bu çalışmada, mikro boşluklu düzlemsel anot/katot elektrot plakalı atmosfer altı basınçta DC -beslemeli gaz deşarj-yarıiletken mikro plazma sistemlerin (GDSµPS) temel karakteristik özellikleri COMSOL Multifizik simülasyon platformunda incelendi. Modelde alüminyum galyum antimonid (AlGaSb) katot elektrot, ITO/SiO$_2$ anot elektrot, 100 µm gaz deşarj aralığına sahip mikro plazma hücresi modellendi. Plazma reaktör ortamında 150 Torr basınç seviyesinde argon (Ar) ve molar %5 hidrojen (H$_2$) argon/hidrojen (Ar/H$_2$) karışımı tanımlandı. Micro plazma hücresi 1.0 kV DC sabit gerilim altında beslendi. Model, elektron yoğunluğu, elektron enerji yoğunluğu, elektron akım yoğunluğu ve elektrik potansiyeli dahil olmak üzere çeşitli deşarj parametrelerinin uzaysal-zamansal dinamiklerini çözerek AlGaSb-Ar/H$_2$ glow deşarj mikro plazma sisteminin geçiş fiziksel özelliklerini anlamak için simüle edildi. Uygulamaya özel hibrit mikro plazma–yarı iletken tabanlı kızılötesi fotodetektör cihazlarının modellenmesinde argona bir miktar hidrojen ilavesinin etkili bir araç olarak kullanılabileceği gözlemlenmiştir.

Anahtar Kelimeler: Mikroplazma, AlGaSb, DC plazma simülasyonu, kızılötesi fotodetektör.

1. INTRODUCTION

The emerging importance of microplasma devices in a wide variety of applications including, electric micropropulsion [1,2], microplasma thruster [3], microplasma materials [4], semiconductor gas discharge-based infrared converter systems [5, 6], biomedical plasma applications in medicine [7,8] requires advanced characterization of the spatiotemporal discharge dynamics of plasma formation at the microscale.

Recent studies were reported on the theoretical and experimental investigation of planar DC field -driven gas discharge-semiconductor micro plasma systems (GDSµPS) [9-11] for modeling high-efficiency infrared-to-visible image converters. An experimental study for self-sustaining DC glow discharges in air and neon gas media coupled with GaAs was reported at both sub- and atmospheric pressures [12]. Electro-optical analyzes of GaAs and GaP photocathode materials in the infrared detector applications have recently been studied [13]. An experimental investigation and a theoretical FEM analysis on electron density, electric potential and breakdown phenomena in a gas discharge medium

consisting of air and helium coupled with InP photocathode material were reported [14]. Numerous theoretical and experimental research and development studies for advanced microplasma devices in diverse fields of science and engineering applications were reported [15-38].

In this study, a number of key operational characteristics of an exclusively-designed DC field -driven microplasma cell were broadly investigated in a 2D simulation platform based on mixture-averaged diffusion-drift theory of gas discharges and Maxwellian electron energy distribution function. The intended microplasma cell structure is basically built of a planar anode/cathode electrode pair, seperated by a gas discharge microgap, and coupled to a high-Ohmic semi-insulating aluminum gallium antimonide (AlGaSb) photocathode material with finely digitated planar electron emission surface. This novel bandgap-tunable infrared material was used in this simulation model due to its high response speed, high sensitivity and efficiency in producing photons in the atmospheric window from 3 μm to 5 μm wavelength range. Furthermore, Al-rich AlGaSb was reported to be more chemically stable and resistant to oxidation than pure AlSb [39, 40]. Introducing the process gas medium in the proposed microplasma cell model in this study, argon was mixed with a maximum molar fraction of 5% hydrogen. The criteria, referred in determining the hydrogen ratio in the mixture, are primarily based on the safety issues that arise when working with hydrogen in the experimental setup under the standard laboratory conditions as ignition can occur at a volumetric ratio of hydrogen to air as low as 4% due to its highest rating on the flammability scale. Thus, hydrogen ratio was limited at 5% in the mixture as a constant parameter, and the other key variable parameters of the model were manipulated. The effects of gas pressure on the spatiotemporal evolution of microplasma system were primarily studied in the range of 150 to 250 Torr. Process gas pressure of discharge medium was then set at 150 Torr in the proposed simulation model after several simulation trials, and also referring to the experimental results reported [41]. The electrical equivalent circuit of the cell was driven at 1.0 kV DC in order to simulate the transitions from field emission state to self-sustained normal glow gas discharge state.

Gas breakdown mechanism is governed by Townsend avalanche criterion in Equation 1.

$$\exp(\alpha.d) - 1 = \gamma_{SE}^{-1} \tag{1}$$

where;

α: Ionization coeficient equal to the number of ions produced per electron in unit length.

d: Discharge gap length.

γ_{SE}: Secondary electron emission (SEE) coefficient, which quantifies the probability of electron emission from the cathode surface upon impact of cations.

Equation 1 reveals that SEE coefficient plays an important role in driving the breakdown mechanism. FEM solver-based spatiotemporal simulation can be a useful tool to predict gas discharge parameters and to perform transient analysis of the breakdown states.

In Figure 1, α ions are attracted to the cathode under high voltage, and upon impact, secondary electrons are ejected from the cathode surface to the discharge gap.
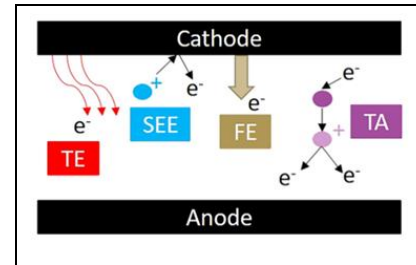
Figure 1. Gas breakdown mechanisms: Thermionic emission (TE), secondary electron emission (SEE), field emission (FE), Townsend avalanche (TA) [22].

Various computational and analytical solutions to these equations for gas breakdown mechanisms were used in recent review articles [11, 18, 19].

A basic 2D-model of GDSμPS cell is introduced with its elemental components in Figure 2.
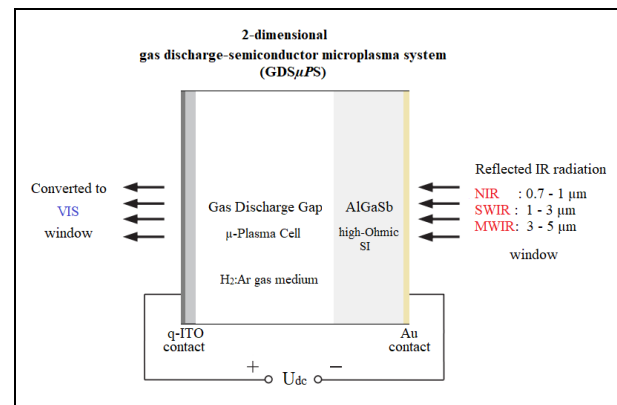
Figure 2. 2D-model of GDSμPS cell.

GDSμPS is principally designed to convert infrared (IR) light to visible (VIS) light in the cell. The incoming IR-light is efficiently absorbed by a wide-bandgap (III-V) and a high-Ohmic (specific resistance, ρ>E5 ohm.cm) semi-insulation cathode material. Electrons are liberated from grounded cathode electrode surface to the gas gap, and accelerated by positively-charged anode electrode. Highly energetic free electrons collide with ion molecules initiating the ionization reactions in the cell. Townsend avalanche (TA) mechanism leads to gas breakdown state, and a normal glow discharge regime is self-sustained by passage of electron current across gas gap under infrared stimulation of photocathode electrode. A characteristic visible glow is emitted from the microplasma cell through a transparent-conductive (ITO) anode electrode.

The antimonide (Sb) -rich III–V compound semiconductors, grown on GaSb or InAs substrates, include GaSb, InAs and AlSb binary compounds [23] with a wide band gap ranging from ~0.1 to ~1.8 eV. The diversity of accessible band alignments in III-Sb

compounds is shown in Figure 3 [24] by which application-specific artificial materials with band gaps from near-infrared (NIR) to far-infrared (FIR) can be designed. The bandgap transitions of binary AlSb/GaSb alloys to ternary III-V compound $Al_xGa_{1-x}Sb$ alloys can be controlled between an indirect band gap AlSb semiconductor with $Eg = 1.62$ eV and a direct band gap GaSb semiconductor with $Eg = 0.72$ eV depending on the specific optoelectronic application [25].
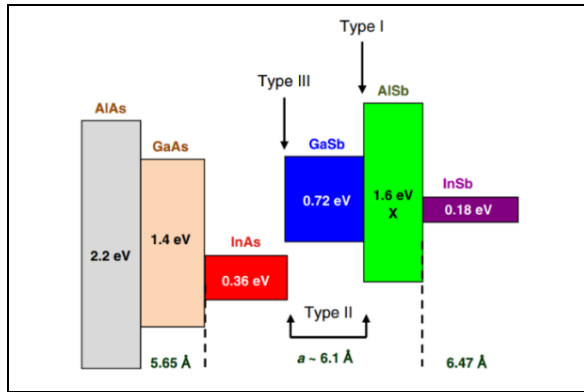
Figure 3. Band alignments of III-As and III-Sb compounds. Scaled boxes represent band gaps of compounds, upper and lower lines of conduction and valence bands, respectively [25].

In Figure 4, a basic physical layout of the microplasma cell model is shown in quadrant-I region of the cylindrical coordinate system (r=x, θ=0, z) in 2D.

In this simulation model, infrared transparent thin Au film -coated planar AlGaSb cathode with digitated electron emission surface was coupled across a gas discharge gap of 100 µm distance to thin ITO film - coated planar anode substrate of SiO_2 fused glass.
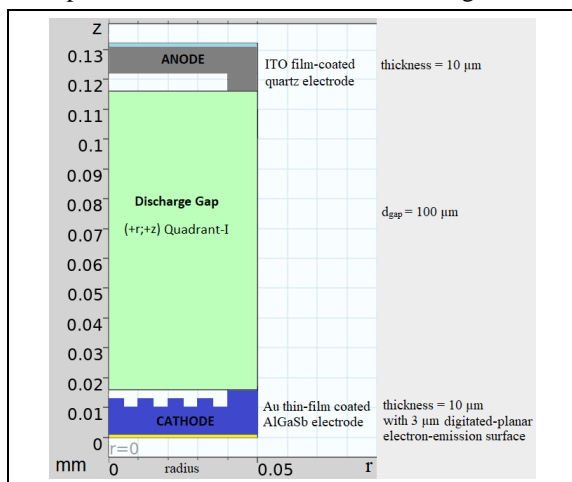
Figure 4. Physical layout of GDSµPS cell model in 2D.

The simulation studies were performed based on boundary-seperated mesh structure as shown in Figure 5.
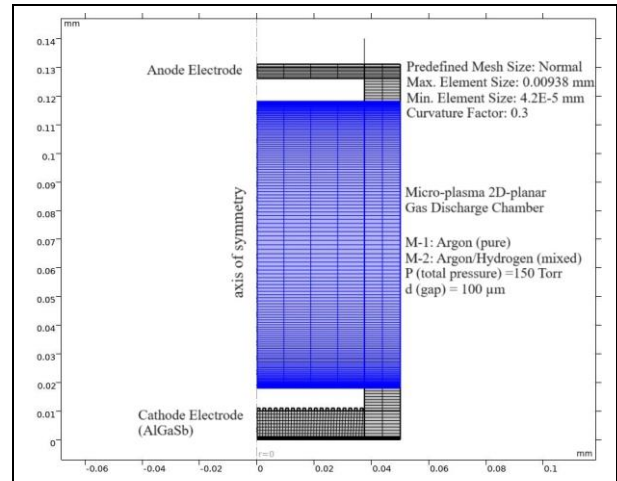
Figure 5. Mesh structure of GDSµPS cell model in 2D.

2. NUMERICAL ANALYSIS

A set of discharge parameters including, electron density (ED), electron energy density (EED), electron current density (ECD), and electric potential (EP) was studied using the COMSOL Multiphysics simulation program based on mixture-averaged diffusion-drift theory of gas discharges and Maxwellian electron energy distribution function.

In this study, the parameters and variables of GDSµPS cell models were set as follows:

i. Voltage supply to drive the cell: V=1.0 kV DC.

ii. Plasma process gas types: Argon (Ar) and argon mixed with molar fraction of 5% hydrogen (Ar/H₂).

iii. Gas pressure: P=150 Torr.

iv. Ambient cell operating temperature: T=300 K.

v. Gas discharge gap length: d = 100 µm.

vi. Cathode electrode: III-antimonide compound high-Ohmic semi-insulating aluminum gallium antimonide (AlGaSb) material.

vii. Modification of cathode electron emission surface: Finely digitated in the formation of 1.0 µm height and 1.0 µm width periodic squares of comb plate style.

viii. Cathode electrode width: w=100 µm, divided by a central symmetry axis in the 2D-model.

ix. Anode electrode: 1.0 µm thick ITO (In₂O₃-SnO₂ indium tin oxide) -coated fused glass (SiO₂) substrate.

x. Initial electron density in the plasma reactor cell: $n_{e,o}$= 1.0E17 (1/m³).

In the discharge model with binary argon-hydrogen gas medium, it is aimed to manipulate the operating point of GDSµPS cell on the imaginary vertical projection line corresponding to P.d=1.50 Torr.cm in the Paschen curve.
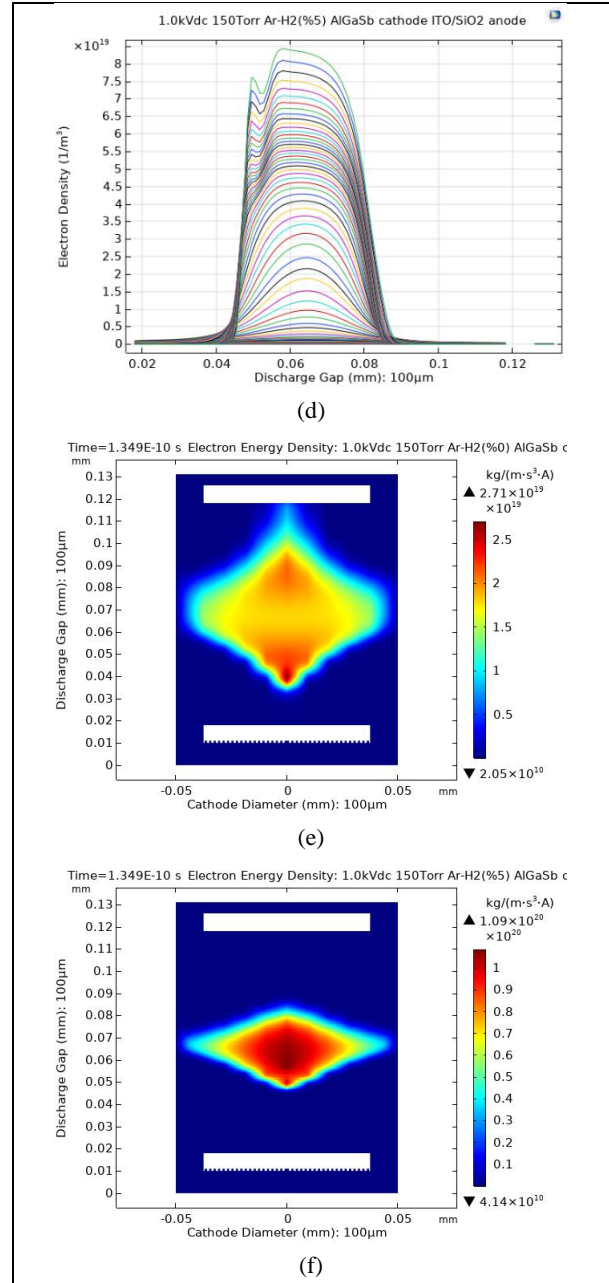
3. RESULTS AND DISCUSION

Figure 6 (a) and (b) show 2D-images of spatiotemporal variation of Electron Density (ED) parameter calculated at final output time (t=1.349E-10s) of the plasma

transition period, respectively for Ar/H$_2$(%0) and Ar/H$_2$(%5) gas media, and displayed in rainbowclassic color range across discharge gap. Figure 6 (c) and (d) show 1D-images of spatiotemporal variation of Electron Density (ED) parameter calculated at full output time range respectively for Ar/H$_2$(%0) and Ar/H$_2$(%5) gas media, and plotted as curves across discharge gap. Figure 6 (e) and (f) show 2D-images of spatiotemporal variation of Electron Energy Density (EED) parameter calculated at final output time respectively for Ar/H$_2$(%0) and Ar/H$_2$(%5) gas media, and displayed in rainbowclassic color range across discharge gap.
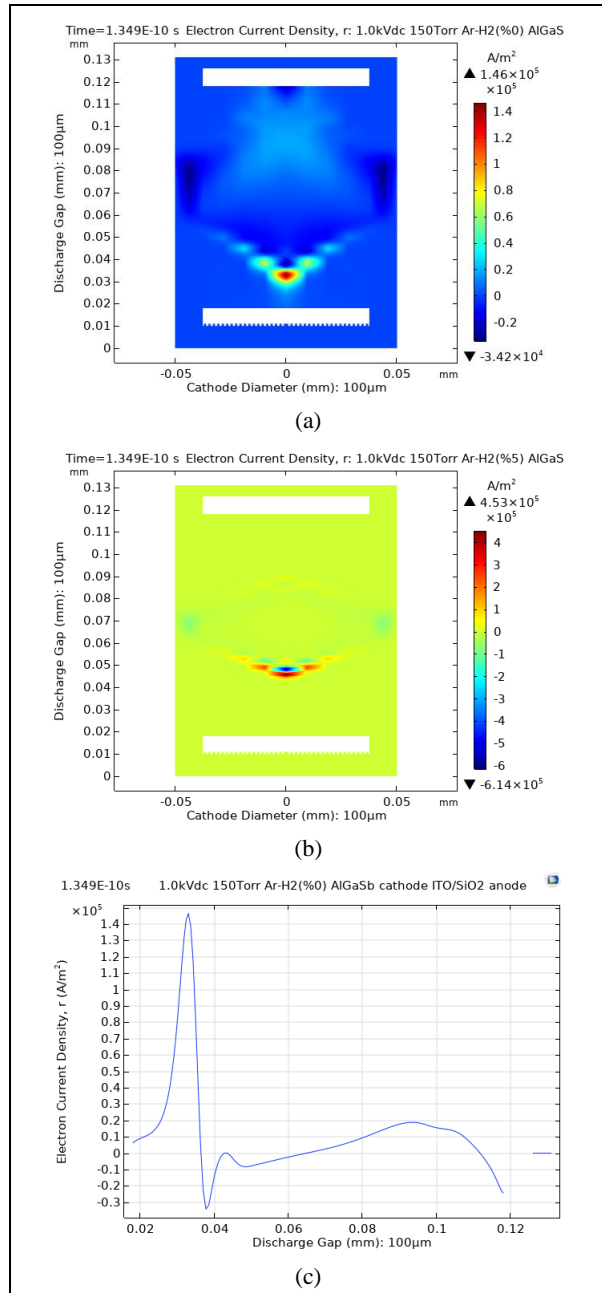

(a)

(b)

(c)
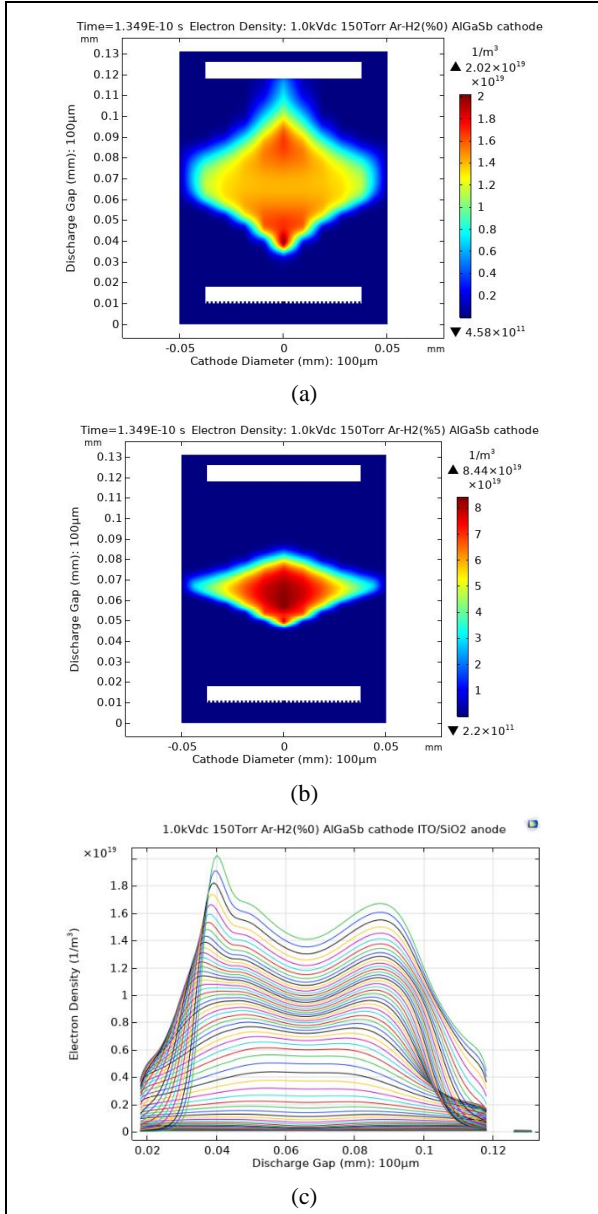
Figure 6. Spatiotemporal simulation of 2D-GDSµPS cell model: (a) 2D image of Electron Density (ED) in Ar/H$_2$(%0) at final output time (t=1.349E-10s) of the plasma transition period, (b) 2D image of Electron Density (ED) in Ar/H$_2$(%5) at final output time (t=1.349E-10s) of the plasma transition period, (c) 1D plot of Electron Density (ED) in Ar/H$_2$(%0) at full output times,

(d)

(e)

(f)

Figure 6 (cont.). (d) 1D plot of Electron Density (ED) in Ar/H$_2$(%5) at full output times, (e) 2D image of Electron Energy Density (EED) in Ar/H$_2$(%0) at final output time (t=1.349E-10s) of the plasma transition period, (f) 2D image of Electron Energy Density (EED) in Ar/H$_2$(%5) at final output time (t=1.349E-10s) of the plasma transition period.

Figure 7 (a) and (b) show 2D-images of spatiotemporal variation of Electron Current Density (ECD) parameter calculated at final output time (t=1.349E-10s) of the plasma transition period, respectively for Ar/H$_2$(%0) and Ar/H$_2$(%5) gas media, and displayed in rainbowclassic color range across discharge gap. Figure 7 (c) and (d) show 1D-images of spatiotemporal variation of Electron Current Density (ECD) parameter calculated at final output time respectively for Ar/H$_2$(%0) and Ar/H$_2$(%5) gas media, and plotted as single curve across discharge

gap. Figure 7 (e) and (f) show 2D-images of spatiotemporal variation of Electric Potential (EP) parameter calculated at final output time respectively for Ar/H$_2$(%0) and Ar/H$_2$(%5) gas media, and displayed in rainbowclassic color range across discharge gap.

(a)

(b)

(c)

Figure 7. Spatiotemporal simulation of 2D-GDSµPS cell model: (a) 2D image of Electron Current Density in Ar/H$_2$(%0) at final output time (t=1.349E-10s) of the plasma transition period, (b) 2D image of Electron Current Density in Ar/H$_2$(%5) at final output time (t=1.349E-10s) of the plasma transition period, (c) 1D plot of Electron Current Density in Ar/H$_2$(%0) at final output time (t=1.349E-10s) of the plasma transition period,
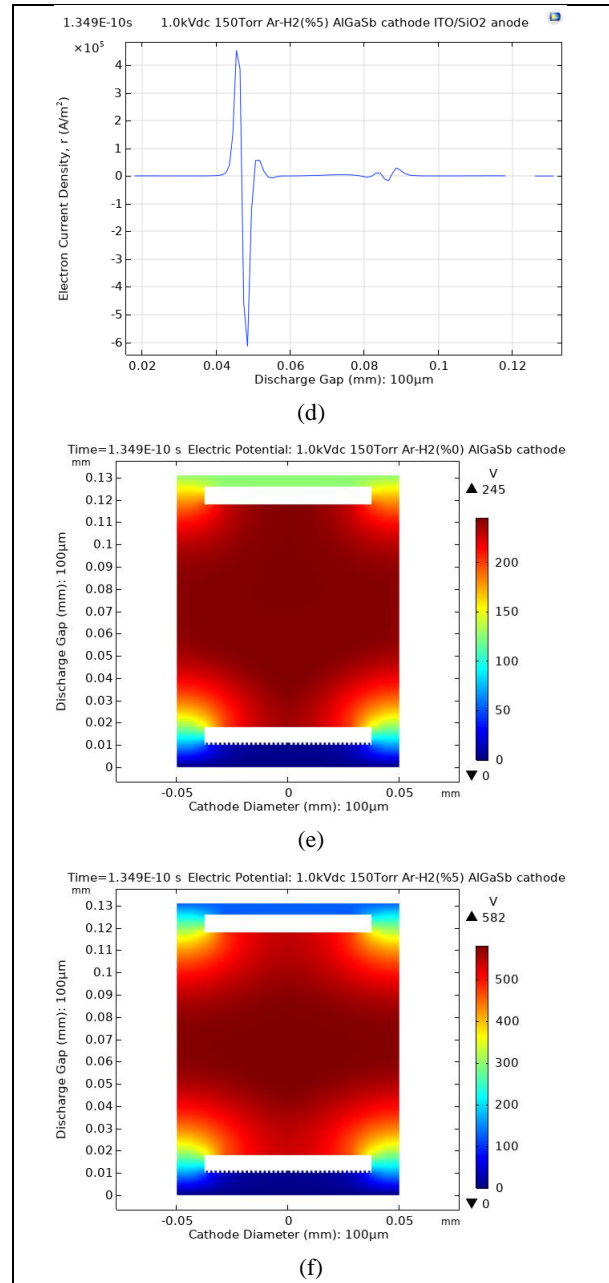

(d)

(e)

(f)

Figure 7 (Cont.). (d) 1D plot of Electron Current Density in Ar/H$_2$(%5) at final output time (t=1.349E-10s) of the plasma transition period, (e) 2D image of Electric Potential in Ar/H$_2$(%0) at final output time (t=1.349E-10s) of the plasma transition period, (f) 2D image of Electric Potential in Ar/H$_2$(%5) at final output time (t=1.349E-10s) of the plasma transition period.

❖ Simulation results based on findings from Figure 6:

• The peak electron density (ED), calculated at final output time (t=1.349E-10s) of the plasma transition period, is higher (approximately x4 times) as displayed in Fig. 6(b) with Ar/H$_2$(%5) than in Fig. 6(a) with Ar/H$_2$(%0).

• The electron density (ED) distribution, calculated at full output time range, is more localized across discharge gap

as displayed in Fig. 6(d) with Ar/H$_2$(%5) than in Fig. 6(c) with Ar/H$_2$(%0).

• The peak electron energy density (EED), calculated at final output time (t=1.349E-10s) of the plasma transition period, is higher and more localized across discharge gap as displayed in Fig. 6(f) with Ar/H$_2$(%5) than in Fig. 6(e) with Ar/H$_2$(%0).

❖ Simulation results based on findings from Figure 7:

• The peak electron current density (ECD), calculated at final output time (t=1.349E-10s) of the plasma transition period, is higher (approximately x3 times) as displayed in Fig. 7(b) with Ar/H$_2$(%5) than in Fig. 7(a) with Ar/H$_2$(%0).

• The electron current density (ECD) distribution, calculated at final output time (t=1.349E-10s) of the plasma transition period, is more localized across discharge gap as displayed in Fig. 7(d) with Ar/H$_2$(%5) than in Fig. 7(c) with Ar/H$_2$(%0).

• The peak electric potential (EP), calculated at final output time (t=1.349E-10s) of the plasma transition period, is higher in value and more localized across discharge gap as displayed in Fig. 7(f) with Ar/H$_2$(%5) at 582 Vdc than in Fig. 7(e) with Ar/H$_2$(%0) at 245 Vdc.

Figure 8 introduces the I-V characteristics of gas discharges including, dark discharge, glow discharge and arc discharge regimes [28, 29].

The operating point of GDSµPS cell model, simulated in this study, is indicated by dashed vertical line in blue corresponding to an estimated current of ~ 0.5 mA in the normal glow discharge regime.
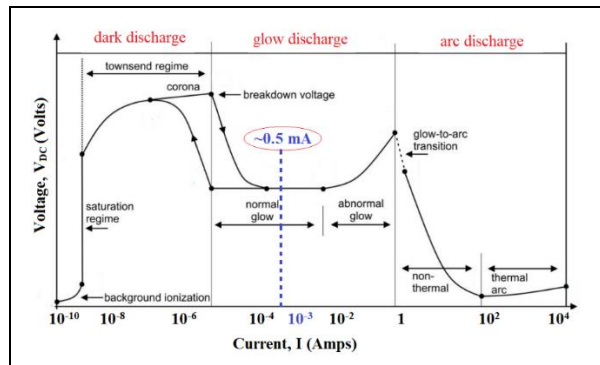
Figure 8. I-V characteristics of gas discharges including, dark discharge, glow discharge and arc discharge regimes [28, 29].

Figure 9 shows Paschen curves for argon and hydrogen gases [29]. It is aimed to locate the operating point of GDSµPS cell on the imaginary vertical projection line corresponding to P.d = 1.50 Torr.cm, and to manipulate it by hydrogen addition to argon.
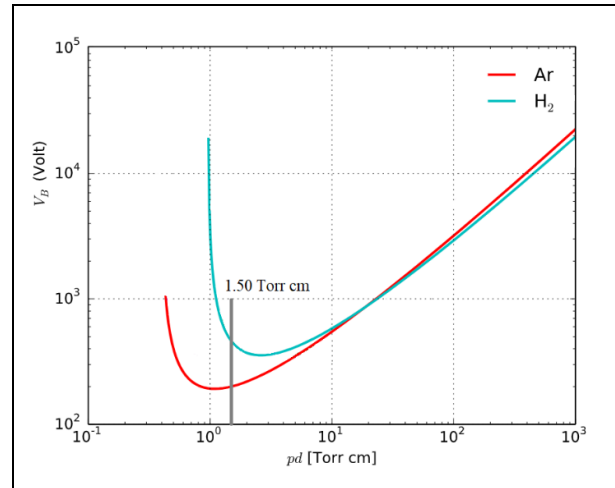
Figure 9. Paschen curves for argon and hydrogen gases [29]. The operating point of GDSµPS cell is located on the imaginary vertical projection line corresponding to P.d = 1.50 Torr.cm.

4. CONCLUSIONS

It is concluded that hydrogen addition to argon can be used as an effective design tool to control the operating point of GDSµPS cell for the dedicated application.

Numerical analysis results are reported as follows:

By hydrogen addition to argon, the operating point of the proposed GDSµPS cell model can be controlled on the imaginary vertical projection line corresponding to P.d=1.50 Torr.cm in the Paschen curve.

The calculated electric potential (EP) at final output time (t=1.349E-10s) of the plasma transition period peaks at 582 Vdc in the binary Ar/H$_2$(%5) gas model and peaks at 245 Vdc in the unary Ar gas model.

The calculated peak electron density (ED) at final output time (t=1.349E-10s) of the plasma transition period is approximately four times higher in the binary Ar/H$_2$(%5) gas model than in the unary Ar gas model.

The calculated peak electron current density (ECD) at final output time (t=1.349E-10s) of the plasma transition period is approximately three times higher in the binary Ar/H$_2$(%5) gas model than in the unary Ar gas model.

Electron density (ED), electron current density (ECD), and electron energy density (EED) distribution patterns are highly localized across discharge gap in the binary Ar/H$_2$(%5) gas model than in the unary Ar gas model at final output time (t=1.349E-10s) of the plasma transition period.

The operating point of GDSµPS cell model locates in the normal glow discharge regime at an estimated current rating of ~ 0.5 mA as calculated.

It is figured out that the binary Ar/H$_2$ gas discharge model can undertake a major role in shaping and controlling the spatiotemporal response to transient electro-optical behavior of microplasma-based artificial electromagnetic materials configured for high-efficiency infrared-to-visible wavelength conversion applications [42-44].

Symbols and Abbreviations

Ar: Argon
H_2:Hydrogen
Au: Gold
ITO: Indium Tin Oxide
SiO_2:Silicon Dioxide, Silica
AlGaSb: Aluminum Gallium Antimonide
GDSµPS: Gas Gischarge-Semiconductor Microplasma System
FEM: Finite Element Method
DC: Direct Current
I-V: Current-Voltage
SEE: Secondary Electron Emission
TE: Thermionic Emission
FE: Field Emission
TA: Townsend Avalanche
VIS: Visible
NIR: Near-infrared
SWIR: Short-wave infrared
MWIR: Mid-wave infrared
FIR: Far-infrared
ED: Electron Density
EED: Electron Energy Density
ECD,r: Electron Current Density (r-component)
EP: Electric Potential.

ACKNOWLEDGEMENT

DECLARATION OF ETHICAL STANDARDS

The authors of this article declare that the materials and methods used in this study do not require ethical committee permission and/or legal-special permission.

AUTHORS' CONTRIBUTIONS

Erhan ONGUN: Modeling, simulation, article writing.

Selçuk UTAŞ: Modeling, simulation.

Prof. Dr. Hatice Hilal YÜCEL (KURT): Supervisor of ONGUN's doctoral thesis, expert on the plasma science and technology, article writing and editing.

Prof. Dr. Aybaba HANÇERLİOĞULLARI: Member of ONGUN's doctoral thesis monitoring committee.

CONFLICT OF INTEREST

There is no conflict of interest in this study.

REFERENCES

[1] Baranov O.O., Xu S., Xu L., Huang S., Lim J.W.M., Cvelbar U., Levchenko I., and Bazaka K., "Miniaturized plasma sources: Can technological solutions help electric micropropulsion?", *IEEE Trans. Plasma Sci.*, 46: 230–238, (2017).

[2] Shivkumar G., Qiao L., and Alexeenko A.A., "Plasma-flow interactions in field-emission discharges with applications in microcombustion," *J. Phys. D Appl. Phys.*, 52: 384001, (2019).

[3] Takahashi T., Mori D., Kawanabe T., Takao Y., Eriguchi K., and Ono K., "Microplasma thruster powered by X-band microwaves", *J. Appl. Phys.*, 125: 083301, (2019).

[4] Chiang W.-H., Mariotti D., Sankaran R.M., Eden J.G., and Ostrikov K., "Microplasmas for advanced materials and devices", *Adv. Mater.*, 32: 1905508, (2020).

[5] Kurt H.H., Koc E., Salamov B.G., "Atmospheric Pressure DC Glow Discharge in Semiconductor Gas Discharge Electronic Devices", *IEEE Transactions on Plasma Science*, 38(2): 137-141, (2010).

[6] Kurt H.H., Tanrıverdi E., "The Features of GaAs and GaP Semiconductor Cathodes in an Infrared Converter System", *Journal of Electronic Materials*, 46: 4024-4033, (2017).

[7] T von Woedtke, Laroussi M. and Gherardi M., "Foundations of plasmas for medical applications", *Plasma Sources Science and Technology*, 31: 054002, (2002).

[8] Laroussi M., "Low-temperature plasma jet for biomedical applications: A review", *IEEE Trans. Plasma Sci.*, 43: 703–712, (2015).

[9] Bülbül M.M., Kurt H.H., Salamov B., "Surface behaviour of plasma etched photodetector in a planar gas discharge image converter", *7th Int'l Conference on Nanometer-Scale Science and Technology*, (2002).

[10] Sadiq Y., Kurt H.Y., Albarzanji A.O., Alekperov S.D, Salamov B.G., "Transport properties in semiconductor-gas discharge electronic devices", *Solid-state electronics*, 53(9): 1009-1015, (2009).

[11] Garner A.L., Loveless A.M., Dahal J.N., and Venkattraman A., "A tutorial on theoretical and computational techniques for gas breakdown in microscale gaps", *IEEE Trans. Plasma Sci.*, 48: 808–824, (2020).

[12] Kurt H.Y., Sadıq Y., Salamov B.G., "Nonlinear electrical characteristics of semi-insulating GaAs", *Physica status solidi (a)*, 205(2): 321-329, (2008).

[13] Kurt H.H., Tanrıverdi E., "Electrical properties of ZnS and ZnSe semiconductors in a plasma-semiconductor system", *Journal of Electronic Materials*, 46: 3965–3975, (2017).

[14] Kurt H.H., Salamov B.G., "Breakdown Phenomenon and Electrical Process in a Microplasma System with InP Electrode", 7th European Conference on Renewable Energy Systems, *JOM*, 72: 651–657, (2020).

[15] Chiang W.-H., Mariotti D., Sankaran R. M., Eden J. G., and Ostrikov K., "Microplasmas for advanced materials and devices", *Adv. Mater.*, 32: 1905508, (2020).

[16] Zhang J. et al., "Engineering Surface Plasmons in Metal/Nonmetal Structures for Highly Desirable Plasmonic Photodetectors", *ACS Materials Lett.*, 4: 343−355, (2022).

[17] Fu Y., Zhang P., Krek J., and Verboncoeur J.P., "Gas breakdown and its scaling law in microgaps with multiple concentric cathode protrusions", *Appl. Phys. Lett.*, 114: 014102, (2019).

[18] Fu Y., Zhang P., Verboncoeur J.P., and Wang X., ***Plasma Res. Express*** 2: 013001, (2020).

[19] Go D.B. and Venkattraman A., "Microscale gas breakdown: Ion-enhanced field emission and the modified Paschen's curve", ***J. Phys. D Appl. Phys.***, 47: 503001, (2014).

[20] Malayter J.R. and Garner A.L., "Theoretical assessment of surface waviness on work function", ***AIP Adv.***, 10: 095110, (2020).

[21] Brayfield II R. S., Fairbanks A.J., Loveless A.M., Gao S., Dhanabal A., Li W., Darr C., Wu W., and Garner A. L., "The impact of cathode surface roughness and multiple breakdown events on microscale gas breakdown at atmospheric pressure", ***J. Appl. Phys.***, 125: 203302, (2019).

[22] Garner A.L., Meng G., Fu Y. et al., "Transitions between electron emission and gas breakdown mechanisms across length and pressure scales", ***J. Appl. Phys.***, 128: 210903, (2020).

[23] Tournié E. et al., "Mid-infrared III–V semiconductor lasers epitaxially grown on Si substrates", ***Science & Applications***, 11: 165, (2022).

[24] Vurgaftman I., Meyer J.R., Ram-Mohan L.R., "Band parameters for III–V compound semiconductors and their alloys", ***J. Appl. Phys.***, 89: 5815–5875, (2001).

[25] Dutta P.S., Bhat H.L., Kumar V., "The physics and technology of gallium antimonide: an emerging optoelectronic material", ***J. Appl. Phys.***, 81: 5821–5870, (1997).

[26] Naresh C. Das, "Tunable infrared plasmonic absorption by metallic nanoparticles", ***J. Appl. Phys.***, 110: 046101, (2011).

[27] Ongun E., Yücel (Kurt) H.H., Utaş S., "DC-driven subatmospheric glow discharges in the infrared-stimulated", ***J. Mater Sci: Mater Electron***, 35: 655, 1-14, (2024).

[28] Vossen J.L., "Thin Film Processes", ***Academic Press, INC.***, New York, (1978).

[29] Tabib-Azar M., Pai P., "Microplasma Field Effect Transistors", ***Micromachines***, 8: 117, (2017).

[30] Liangliang L., and Wang Q., "Microplasma: A New Generation of Technology for Functional Nanomaterial Synthesis", ***Plasma Chem Plasma Process***, 35: 925–962, (2015).

[31] Kurt H.Y., Salamov B.G., and Mammadov T.S., "Electrical instability in a semiconductor gas discharge system", ***Crystal Research and Technology***, 40(12): 1160-1164, (2005).

[32] Kurt H.Y. Inalöz A., and Salamov B.G., "Study of non-thermal plasma discharge in semiconductor gas discharge electronic devices", ***Optoelectronics and Advanced Materials-Rapid Communications***, 4: 205-210, (2010).

[33] Zimmermann S., Haase M., Lang N., Röpcke J., Schulz S.E., Otto T., "The role of plasma analytics in leading-edge semiconductor technologies", ***Contributions to Plasma Physics***, 58(5): 367-376, (2018).

[34] Choi E.H., Kaushik N.K., Hong Y.J., Lim J.S., Choi J.S., and Han I., "Plasma bioscience for medicine, agriculture and hygiene applications", ***Journal of the Korean Physical Society***, 80: 817–851, (2022).

[35] Kurt H.Y., Kalkan G., Özer M., Tanrıverdi E., Yigit D., "The Effect of the Oxidation on GaAs Semiconductor Surface to the System Characteristics in a Double-Gapped Plasma Cell", ***Journal of Polytechnic***, 17(4): 161-165, (2014).

[36] Kurt H.Y., Sadiq Y., Salamov B.G., "Nonlinear electrical characteristics of semi-insulating GaAs", ***Physica status solidi (a)***, 205(2): 321-329, (2008).

[37] Schoenbach K.H. and Becker K., "20 years of microplasma research: A status report", ***Eur. Phys. J. D***, 70: 29, (2016).

[38] Ünal İ., Karatay S., Yesil A., Hançerlioğulları A., "Seasonal variations of impedance in the ionospheric plasma", ***Journal of Polytechnic***, 23(2): 427-433, (2020).

[39] Bennett, B.R., Khan, S. A., Boos, J.B., Papanicolaou, N. A., Kuznetsov, V. V., "AlGaSb Buffer Layers for Sb-Based Transistors", ***Journal of Electronic Materials***, 39(10): 2196–2202, (2010).

[40] Bennett, B.R., Boos, J.B., Ancona, M.G., Papanicolaou, N. A., Cooke, G. A., Kheyrandish, H., "InAlSb/InAs/AlGaSb Quantum Well Heterostructures for High-Electron-Mobility Transistors", ***Journal of Electronic Materials***, 36(2): 99–104, (2007).

[41] Kurt, H.H., "Exploration of the infrared sensitivity for a ZnSe electrode of an IR image converter", ***Journal of Electronic Materials***, 47(8): 4486-4492, (2018).

[42] Yücel H.H., Utaş S., Ongun E., "The study of DC- and AC-driven GaAs-coupled gas discharge micro plasma systems: Modeling and simulation", ***Journal of Electronic Materials***, 53: 3792-3808, (2024).

[43] Yücel H.H., Utaş S., Ongun E., "The investigation of direct current microdischarges in HgCdTe-coupled Ar/H2 gas medium at atmospheric and hyper-atmospheric pressures", ***Optoelectronics and Advanced Materials – Rapid Communications***, 18(5-6): 296-304, (2024).

[44] Ongun E., Yücel H.H., "Spatiotemporal modeling and simulation of DC microplasma glow discharges in ZnSe-Ar/H2 system", ***Inspiring Technologies and Innovations***, 3(1): 1-8, (2024).